Solvothermal Synthesis and Photocatalytic Performance of Mg^{2+}-Doped Anatase Nanocrystals with Exposed {001} Facets

[a]Maria-Veronica Sofianou, [a]Maria Tassi, [a]Nikos Boukos, [a]Stavros Thanos, [b]Tiverios Vaimakis, [c]Jiaguo Yu, [a]Christos Trapalis*

[a]Institute of Advanced Materials, Physicochemical Processes, Nanotechnology and Microsystems, National Center for Scientific Research "Demokritos", 153 10 Attiki, Greece

[b]Department of Chemistry, University of Ioannina, 451 10, Ioannina, Greece

[c]*State Key Laboratory for Advanced Technology Materials Synthesis & Processing , Wuhan University of Technology, Wuhan 430070, People's Republic of China*

*Dr. C. Trapalis

Institute of Advanced Materials,

Physicochemical Processes,

Nanotechnology and Microsystems,

NCSR "Demokritos",

153 10 Ag. Paraskevi

Attikis, Greece

Tel.: +30 210 650 3343

Fax: +30 210 651 9430.

Email: trapalis@ims.demokritos.gr

Abstract

The photocatalytic activity of TiO_2 and magnesium doped TiO_2 nanocrystals in dopant range of 2-6.2 at%, was studied. The doped and undoped nanocrystals with exposed {001} crystal facets were synthesized by a solvothermal method. Several studies have shown that the (001) surface of the TiO_2 anatase crystal is more reactive than the thermodynamically stable (101) surface. The crystal structure as well as the shape of the TiO_2 and Mg^{2+}/TiO_2 anatase nanoparticles were determined using two different techniques, such as X-ray powder difraction (XRD) and transmission electron microscopy (TEM), which both lead to the agreeable conclusion that the nanocrystals are in the form of plates. Chemical analysis of the photocatalyst was carried out with X-ray photoelectron spectroscopy (XPS) and showed the presence of magnesium ions in the TiO_2 nanoplates. UV-visible diffuse reflectance spectroscopy (DRS) showed that there is an adsorption shift for doped TiO_2 to visible light region.

The photocalaytic efficiency of the synthesized catalysts was investigated by the photocatalytic oxidation of the gaseous nitric oxide (NO) and decomposition of the gaseous acetaldehyde (CH_3CHO) under UV irradiation. It was demonstrated that the low Mg^{2+} doped catalysts exhibited higher photocatalytic activity than the pure TiO_2. The optimal concentration of dopant that is beneficial for the photocatalytic activity was studied.

Keywords*:* TiO_2; Anatase nanoplates; {001} facets; Photocatalysis; NO oxidation; Acetaldehyde decomposition

1. Introduction

Titanium dioxide (TiO_2) is a widely studied semiconductor due to its variable applications, used as a photocatalyst, photovoltaic, sensors and photonic crystal [1-4]. Anatase, rutile and brookite are three crystal polymorphs of TiO_2. From these three phases mentioned, anatase has, in most cases, higher photocatalytic activity than the other ones [5-7]. It is well known that the photocatalytic activity of TiO_2 depends partially on the recombination rate of the photogenerated electron and hole pairs. In order to overcome this limitation, many attempts have been made by modifying TiO_2 with selective surface treatments for example doping with metal ions (transition metal, rare earth metal and noble metal ions), dye photosensitization on its surface, deposition as well as photodeposition of noble metals, etc [8-11]. Studies for modifying TiO_2 by alkaline-earth doping are seldom reported. Moreover, several theoretical and experimental studies have shown that the (001) surface of the anatase crystal is more reactive than the (101) surface [12-14]. This implies that TiO_2 structures with exposed {001} crystal facets doped with alkaline-earth ions will achieve high photocatalytic activity. This study presents the synthetic procedure of magnesium ion doped TiO_2 anatase products with exposed highly reactive {001} crystal facets and evaluates the influence of the structure and the percentage of dopant in their photocatalytic activity in decomposing the acetaldehyde gas and oxidizing the NO gas, which both are prominent air pollutants. The photocatalytic activity of the different anatase structures is evaluated by comparing their photonic efficiencies that were calculated from the amount of the acetaldehyde gas decomposed and NO gas oxidized to NO_2 and NO_3^-.

2. Experimental

2.1. Synthesis of Mg^{2+}/TiO_2 anatase samples

TiO_2 nanoplates and Mg^{2+}/TiO_2 anatase nanocrystals with exposed {001} crystal facets were prepared using a solvothermal method. In a typical synthesis for TiO_2 anatase nanoplates, 3 mmol of titanium isopropoxide [$Ti(C_3H_7O)_4$] from Alfa Aesar Chemicals were dissolved into 50 ml of absolute ethanol from Merck under vigorous stirring at room temperature. 0.6 ml (0.03 mol) of hydrofluoric acid (HF 40%) from Merck were added into the above solution as a capping agent in order to achieve the dominant formation of the {001} facets of the anatase crystal. Then the solution was poured into a 60 ml Teflon-lined autoclave until 80% of its volume was filled and was placed into the oven for 24 h at 180 °C. The as-synthesized powder product was collected through centrifugation of the solution. In order to obtain fluoride free TiO_2 anatase nanoplates, with no adsorbed fluoride atoms on their {001} crystal facets, the collected powder product was washed 3 times with distilled water and then was dispersed in 50 ml of 5 M NaOH aqueous solution and stirred for approximately 30 min. Then the dispersion was centrifuged and washed several times until the pH reached 7 and was dried in a furnace at 70 °C overnight. For the preparation of Mg-doped TiO_2 anatase nanocrystals, the same procedure was followed and a concentration of magnesium nitrate [$Mg(NO_3)_2 \cdot 6H_2O$ 99%] from Merck was added to the calculated amount of TiO_2 in order to get the dopant concentration within the range of 2-6 at%.

2.2. Characterization techniques

The crystalline phase of the pure TiO_2 and Mg^{2+}/TiO_2 anatase samples was investigated by X-ray diffractometry (SIEMENS D500 diffractometer) using CuKα radiation. The measurements were performed using the following combination of slits: 1.0°/1.0°/1.0° as aperture diaphragms, 0.15° as detector diaphragm, and 0.15° as diffracted beam monochromator diaphragm. The measured 2θ range between 20° and 100° was scanned in steps of 0.03°/10s. The accelerating voltage and applied current were 40 kV and 35 mA, correspondingly. The identification of the patterns was done with the cards of the International Centre for Diffraction Data. The shape and the crystal structure were observed with a transmission electron microscope (Philips CM20) operated at 200 kV and equipped with a Gatan GIF200 image filter. The TEM specimens of the TiO_2 anatase structures were prepared by direct deposition on a carbon coated Cu TEM grid. Chemical analysis of the Mg/TiO_2 anatase nanoplates were carried out with X-ray photoelectron spectroscopy (XPS) in an ultra-high vacuum VG ESCALAB 210 electron spectrometer equipped with a multichannel detector. The spectra were excited using Mg Kα (1253.6 eV) radiation (operated at 200 W) of a twin anode in the constant analyzer energy mode with pass energy of 30 eV. All the binding energies were referred to the C 1s peak at 284.8 eV and to the O 1s peak at 530.2 eV of the surface adventitious carbon and oxygen respectively. UV-vis diffuse reflectance spectra of all samples were obtained from the dry-pressed film samples using a UV-vis spectrometer (UV-2100, Shimadzu, Japan) with an integrating sphere attachment for their reflectance in the wavelength range 200-900 nm. $BaSO_4$ was used as a reflectance

standard. The widths of the effective band gaps of the samples were determined using Kubelka-Munk phenomenological theory. The theoretical study of the energy band gap of the Mg-doped anatase structures of TiO_2 was performed using the Density-Functional Theory (DFT) [15, 16] and the numerical calculations were implemented with the Quantum Espresso code [17]. The Kohn-Sham wave functions were expanded into a plane wave basis set with an energy cutoff of 32 Ryd. Additionally, the Vanderbilt ultrasoft pseudopotentials calculated with Perdew–Zunger (PZ) exchange-correlation functional were used, while for Mg the Von Barth-Car norm-conserving pseudopotential calculated with Perdew–Zunger (PZ) exchange-correlation functional was employed. Also, the Local Density Approximation (LDA) [18] with Hubbard, factor U, correction (LDA+U) was used in order to obtain the improvement of band structure. The factor U was chosen to be 8 eV. The proper choice has been made after the calculation of the energy band gap of anatase with different values of U, and it was found that, for this value, the evaluated band gap is 3.24 eV, which is close to the experimental value 3.239 eV [19].

2.3 Evaluation of the photocatalytic activity

The photocatalytic activity of the TiO_2 and Mg^{2+}/TiO_2 anatase samples was studied in the oxidation of the NO gas following the ISO standard ISO/DIS 22197-1 and in the acetaldehyde gas decomposition [20]. The as-prepared samples were pressed in sample holders with an apparent surface area of 20 cm^2 and then were pre-illuminated under a UV-A lamp with a light irradiance of 10 W/m^2 for three days in order to remove all possible organic

residual compounds from the sample's surfaces. After the pre-illumination period the sample holders containing the TiO_2 and Mg^{2+}/TiO_2 powders were placed into the flow-type photoreactor with their surface parallel to an optical quartz window and were illuminated by UV-A radiation. The sample holders were separated from the window by a 5 mm thick air layer. The test gas passed only through the space between the sample holder and the window. The reactor is fabricated from materials that adsorb minimal NO or acetaldehyde gas and withstand irradiation of near-UV light. The TiO_2 and Mg^{2+}/TiO_2 anatase samples were exposed to model air containing 1 ppm nitric oxide (NO) or 30 ppm acetaldehyde (CH_3CHO). The photocatalyst adsorbs and oxidizes the NO to NO_2 and NO_3^- on its surface. In the case of the acetaldehyde it is also adsorbed on the photocatalyst surface and then decomposed. The performance of the photocatalyst is determined by the amount of the net removal of the nitrogen oxide (NO) and of the acetaldehyde. The adsorption and desorption of the NO gas on the surface of the photocatalyst was evaluated by monitoring the concentration of the gas in the dark. The photocatalytic activity of the samples was evaluated under UV-A light illumination with irradiance of 10 W/m^2 for 60 minutes. The photonic efficiency ζ (%) of the TiO_2 and Mg^{2+}/TiO_2 anatase samples for the NO oxidation/acetaldehyde decomposition was calculated using the Eq. (1):

$$\zeta = \frac{n_{\deg raded\ molecules}}{n_{available\ photons}} = \frac{\int_{t_0}^{t_1} AX[ppm]dt}{q_{n,p}\Delta T} \times 100\% \quad (1)$$

where, t_0 is the time moment when UV-A light was switched on, t_1 is the time moment at the end of the illumination, ΔT is determined by equation $\Delta T = t_1 - t_0$, A is the coefficient taken as a product of the gas flow value (3 $L \cdot min^{-1}$ for NO

and 1 L·min^{-1} for acetaldehyde) and of the value 10^{-6} expressed in mol·sec^{-1} (A=2.08x10^{-9} mol·sec^{-1} for NO and A=0.69 x10^{-9} mol·sec^{-1} for acetaldehyde), *X* (taken in ppm) is either the difference between the initial NO/NO_x concentration (~ 1 ppm) and the monitored NO/NO_x concentration or the directly monitored NO_2 concentration. In the case of the acetaldehyde it is the difference between the initial acetaldehyde concentration (~ 30 ppm) and the monitored acetaldehyde concentration. Lastly, $q_{n,p}$ is the photon flux of the samples' surface S (expressed in mol·s^{-1}):

The photon flux of the sample's surface (mol·s^{-1}) can be calculated using the Eq. (2):

$$q_{n,p} = \frac{E\lambda S}{N_A hc}, \qquad (2)$$

where, *E* is the irradiance (W/m^2), *S* is the apparent surface area (m^2), λ is the wavelength (m), N_A is the Avogadro constant (mol^{-1}), *h* is Planck's constant (J·s) and *c* is the speed of light (m/s).

The rate of the gas flow, with 50% relative humidity, into the flow-type photoreactor was 3 L·min^{-1} for the NO gas and 100 mL·min^{-1} for the acetaldehyde gas. The photonic efficiency of the monitored NO, NO_2, NO_x, acetaldehyde gases was calculated at the end of the illuminating period of time. The photocatalytic activity of Evonik Degussa P25 was also measured as a reference.

3. Results and discussion

3.1. Phase observations

The XRD patterns of the TiO_2 and Mg^{2+}/TiO_2 samples are presented in Figure 1. It can be seen that the crystalline phase is anatase [JSPDS No. 021-1272 card] without any impurities of the remaining precursor used each time or the formation of another phase such as rutile or brookite. This observation also indicates that the Mg^{2+} ions are well dispersed in the TiO_2 nanocrystals and did not influence their crystal patterns. Anisotropic growth of the crystals along the c-axis of the anatase lattice is evident by the peak broadening of the (004) reflection and the narrower peak of the (200) reflection. This peak broadening that corresponds to all (00c) reflections is due to the very small dimension of the c-axis where as, in the contrary, the peaks that are related to the (a00) reflections are very narrow as the dimension of the a-axis is bigger [21-23]. This indicates that the (001) surface of the TiO_2 anatase crystal is larger than the (101) surface and the crystals are in the form of plates.

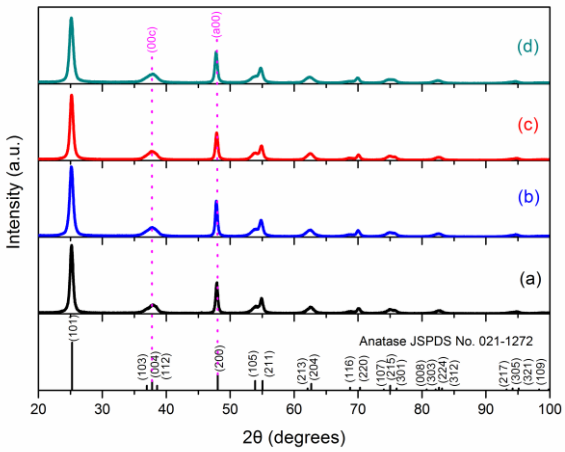

Fig. 1. XRD patterns of the pure TiO_2 anatase nanoplates (a), 2 at% Mg^{2+}/TiO_2 (b), 5.1 at% Mg^{2+}/TiO_2 (c), 6.2 at% Mg^{2+}/TiO_2 anatase nanocrystals (d).

3.2. Morphological observations

The TEM micrographs of the pure and Mg^{2+} doped TiO_2 anatase nanocrystals are presented in Figures 2 (a-h). The large square surface areas of the pure nanoplates are the {001} crystal facets and the small isosceles trapezoidal surfaces are the {101} crystal facets (Fig. 2(a.b)). The corresponding SAED pattern (Fig 2(a) insert) confirms that the square shaped plane is a single crystal, with zone axis [001]. Hence the faceted surface is the (001) surface. After the crystal growth process of the anatase nanocrystals, doped with magnesium ions, the morphological structure of the nanoplates completely changed. More specifically, the nanoplates have become larger and are pilled one on top of the other forming this way a separate bigger nanocrystal (Fig. 2(c,d)). The density of the packed nanoplates is higher on the periphery of the new fabricated nanocrystal, as the color is darker, in comparison to the middle section of the nanocrystal (Fig.2(d)). The corresponding SAED pattern (Fig.2(d) insert) shows that nanoplates are perfectly aligned one on top of the other forming by this way a single crystal. As the content of magnesium ions as dopants in the anatase lattice increases more nanoplates pile up making the crystal more dense and thicker (Fig.2(e,f)). The corresponding SAED pattern (Fig.2(f) insert) shows that the nanoplates are beginning to lose their perfect alignment and the fabricated crystal does not represent a perfect single crystal. With the further increase of Mg^{2+} content in the anatase lattice the nanoplates are densely stocked together forming a sea-urchin morphological structure (Fig.2(g,h)). The corresponding SAED pattern shows that the nanoplates are randomly oriented one on top of the other (Fig.2(h) insert).

It is known from literature that the radius of Mg^{2+} (65 pm) is only slightly smaller than that of Ti^{4+} (68 pm) [23,24]. As a result the Mg^{2+} ion could easily enter into the lattice of the TiO_2 and further replace the Ti^{4+} site and it is therefore introduced substitutionally into the lattice, although there is no direct evidence of this matter [25]. As a Mg^{2+} replaces a Ti^{4+} site, the following reaction takes place:

$$MgO + \frac{1}{2}O_2 \overset{TiO_2}{\uparrow} Mg_{Ti}'' + 2h + 2O_0^x \qquad (3)$$

Where Mg_{Ti}'' is the substitution of a Mg^{2+} in a Ti^{4+} lattice site, O_0^x represents O^{2-} in a normal lattice site. Therefore, when a Mg^{2+} replaces a Ti^{4+} site, the hole density of Mg^{2+} doped TiO_2 increases and the electron density decreases.

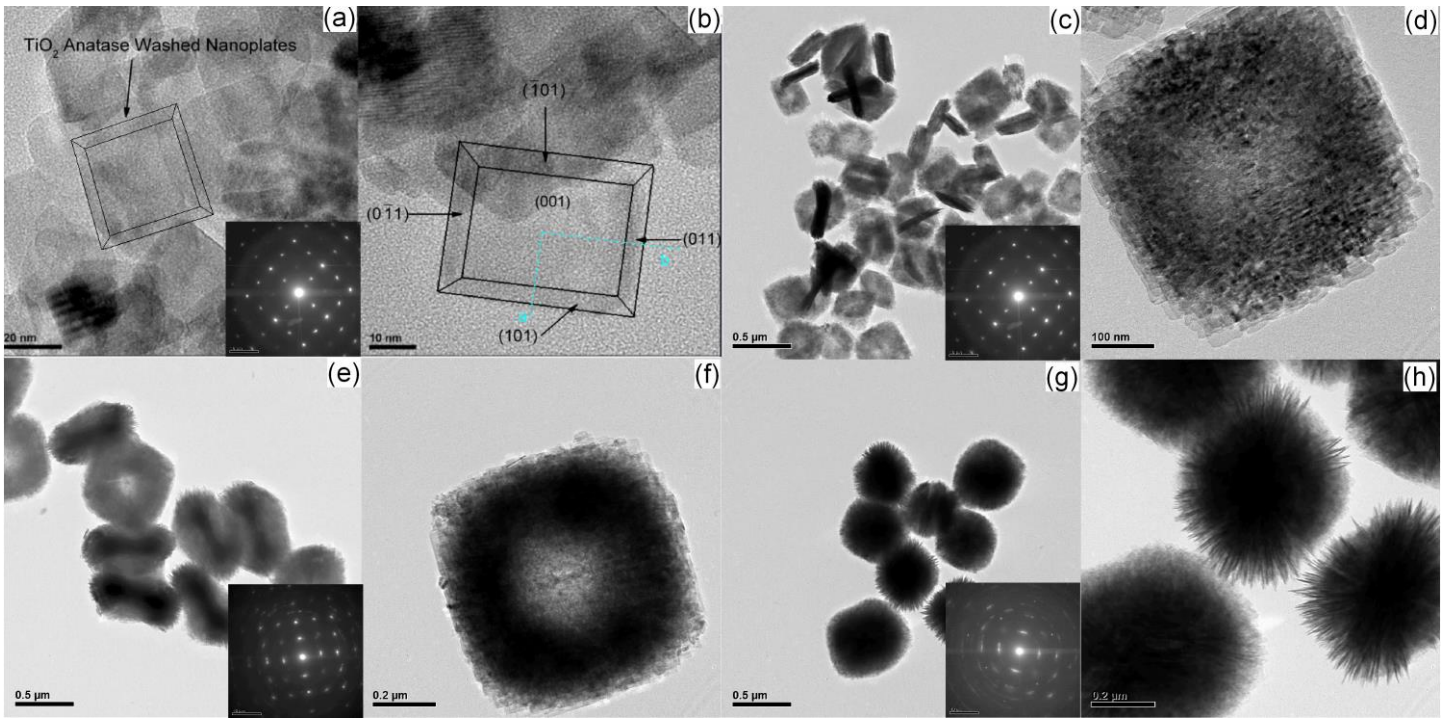

Fig. 2. TEM micrographs of the pure TiO_2 anatase nanoplates, in the insert corresponding SAED pattern (a,b), 2 at% Mg^{2+}/TiO_2, in the insert corresponding SAED pattern (c,d), 5.1 at% Mg^{2+}/TiO_2 in the insert

corresponding SAED pattern(e,f), 6.2 at% Mg^{2+}/TiO_2 anatase nanocrystals, in the insert corresponding SAED pattern (g,h).

3.3. XPS Analysis

XPS measurements were carried out to confirm the presence of magnesium for the sample with the smallest amount of Mg^{2+} ions (2 at% Mg^{2+}/TiO_2) and the high resolution scans are presented in Figure 3. The XPS observations show that only O, Ti, Mg elements were detected from the samples in spectrum analysis. The peak at 530.3 eV (Fig.3(a)) was assigned to the lattice oxygen bonds. The spectra in Figure 3(b) show that the Ti $2p_{1/2}$ and Ti $2p_{3/2}$ peak correspond to the binding energies at 464.98 eV and 459.8 eV respectively. These peaks are attributed to Ti^{4+}. It is reported the binding energies of Ti $2p_{1/2}$ and Ti $2p_{3/2}$ of pure TiO_2 samples are located at 464.0 eV and 458.4 eV correspondingly [26,27]. The slightly positive shift for the Mg^{2+}/TiO_2 sample is due to the presence of magnesium in the anatase lattice [27]. The peak at 51.5 eV (Fig. 3(c)) was assigned to the binding energy of Mg 2p, where Mg^{2+} bonds to oxygen. No fluoride binding energy peak was evident in the sample which indicates that the adsorbed fluoride atoms on the {001} crystal facets were entirely removed during their surface cleaning procedures with a NaOH washing aqueous solution.

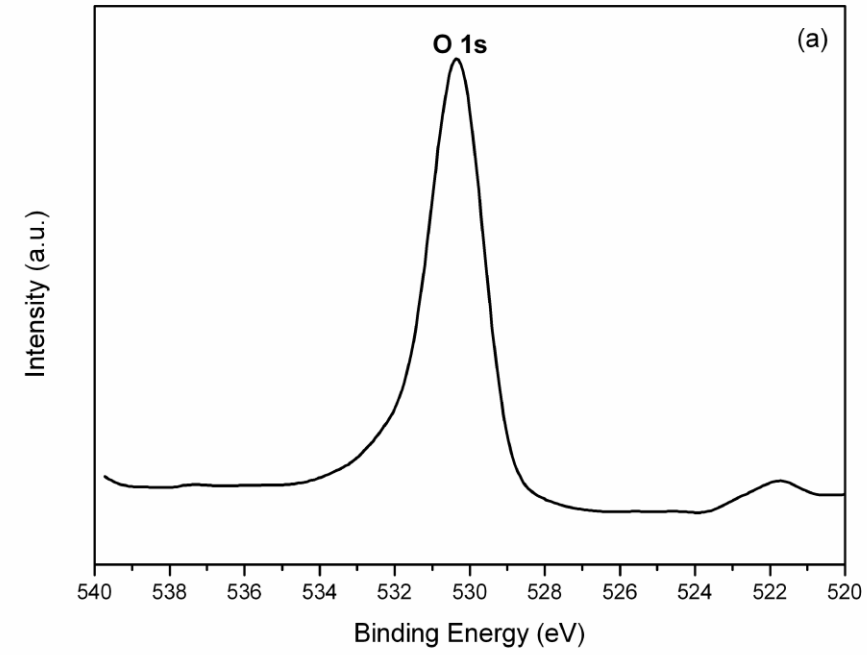
O 1s
(a)
Intensity (a.u.)
540
538
536
534
532
530
528
526
524
522
520
Binding Energy (eV)

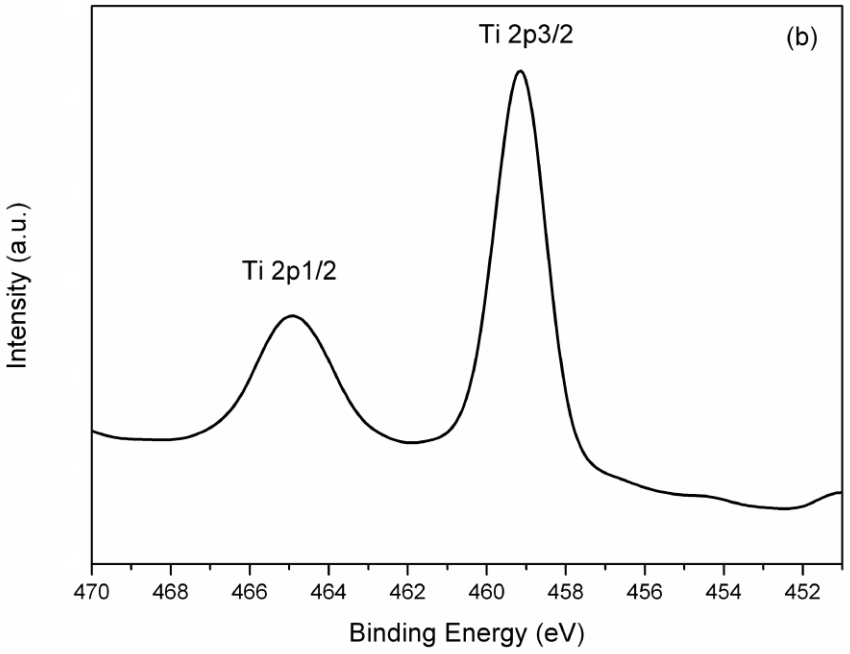
Ti 2p3/2
(b)
Ti 2p1/2
Intensity (a.u.)
470
468
466
464
462
460
458
456
454
452
Binding Energy (eV)

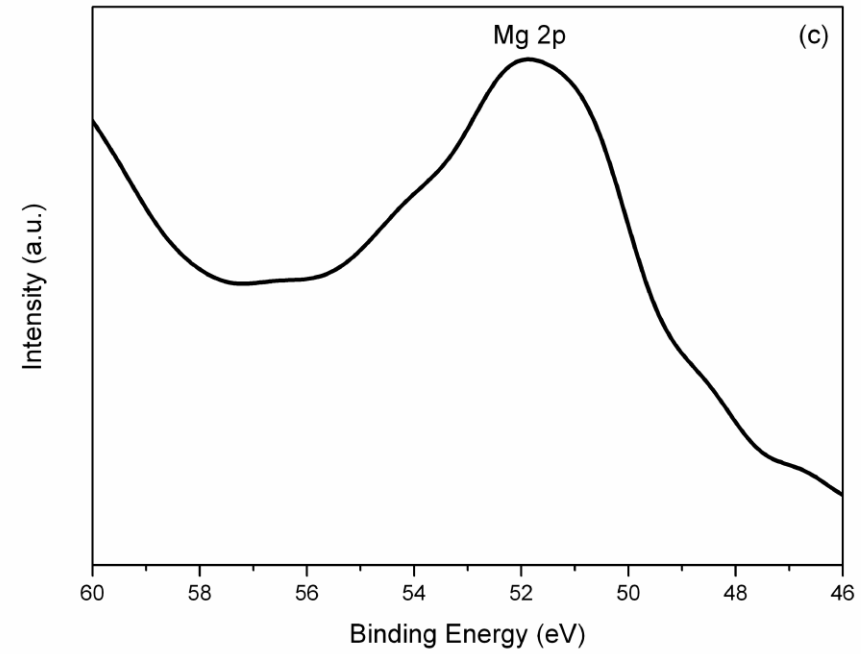
Mg 2p
(c)
Intensity (a.u.)
60
58
56
54
52
50
48
46
Binding Energy (eV)

Fig. 3. High-resolution XPS spectrum of O 1s (a), Ti $2p_{1/2}$, $Ti2p_{3/2}$ (b) and Mg 2p (c) of the sample containing the smallest amount of magnesium (2 at% Mg^{2+}/TiO_2).

3.4. UV-vis spectra

The determination of the band gap of the samples was evaluated using the Kubelka-Munk method based on the diffuse reflectance spectra [28]. The $(F(R)*E)^{1/2}$ versus E(eV) plots of the samples are presented in Figure 4, where $F(R) = (1-R)^2/2R$, R is the diffuse reflectance of the sample relative to the reflectance of the standard $BaSO_4$. The band gap energies Eg were obtained by extrapolating the linear portion (F(R)=0) of the curve onto the x-axis. As can be seen the pure anatase nanoplates absorb around 400 nm due to the band gap absorption of anatase TiO_2, which is ~3.2 eV. More specifically, the pure anatase crystals have an energy gap at 3.23 eV (Fig. 4 (a)), the 2 at% Mg^{2+}/TiO_2 anatase nanocrystals at 3.20 eV (Fig.4(b)), the 5.1 at% Mg^{2+}/TiO_2 anatase nanocrystals at 3.08 eV (Fig.4(c)) and last the 6.2 at% Mg^{2+}/TiO_2 anatase nanocrystals at 3.06 eV (Fig.4(d)).

In order to carry out the theoretical calculations of the energy gap of all crystals the following actions were made. The structures were modelled using supercells of anatase in which a Mg^{2+} ion, in different proportions, was substituted with a Ti^{4+} ion. Specifically, 4, 5, and 12 cells were used in order to achieve ionic ratios of Mg^{2+}/Ti^{4+} such as 1/16 (6.2 at% Mg^{2+}/TiO_2), 1/20 (5.1 at% Mg^{2+}/TiO_2) and 1/48 (2 at% Mg^{2+}/TiO_2) respectively. The lattice parameters were a=b=3.785 Angstroms and c=38.056, 47.57 and 114.168 Angstroms for the 4, 5, and 12 cells respectively. Before the calculation of the

density of states and the energy band gap, the crystal structures were optimized and it was noticed that around the area of Mg, the Ti atoms were moved closer to it, while the O atoms were moved away from it and went closer to the Ti atoms. The distances between the atoms before the geometry optimization for Ti-Mg was 3.040 Å, for O-Mg were 1.964 and 1.973 Å, finally for O-Ti were 1.964 and 1.973 Å. The distances between the atoms after the geometry optimization for Ti-Mg was 3.017 Å, for O-Mg were 2.139 and 1.939 Å, finally for O-Ti were 1.928 and 1.904 Å. Finally, the calculation of density of states and the energy band gap were obtained. More specifically, the calculated energy gap for the pure TiO_2 anatase nanoplates, the 2 at% Mg^{2+}/TiO_2, the 5.1 at% Mg^{2+}/TiO_2 and for the 6.2 at% Mg^{2+}/TiO_2 nanocrystals was 3.24 eV, 3.23 eV, 3.10 eV and 3.05 eV respectively. Figure 5 represents their density of states for the valence and conduction bands. As the concentration of Mg^{2+} in the nanocrystals increases, their band gap decreases and is shifted slightly to the visible light region.

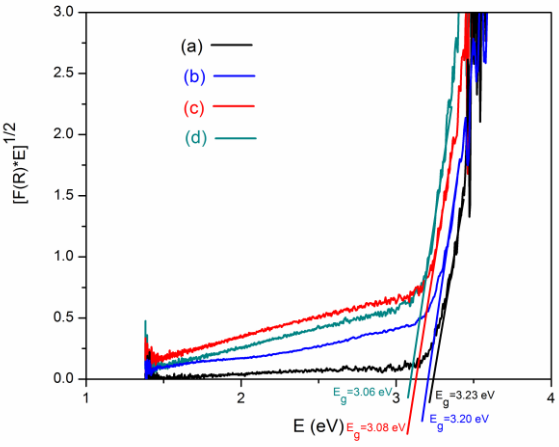

Fig. 4. $(F(R)*E)^{1/2}$ versus E(eV) plots of the pure TiO_2 anatase nanoplates (a), 2 at% Mg^{2+}/TiO_2 (b), 5.1 at% Mg^{2+}/TiO_2 (c), 6.2 at% Mg^{2+}/TiO_2 anatase nanocrystals (d).

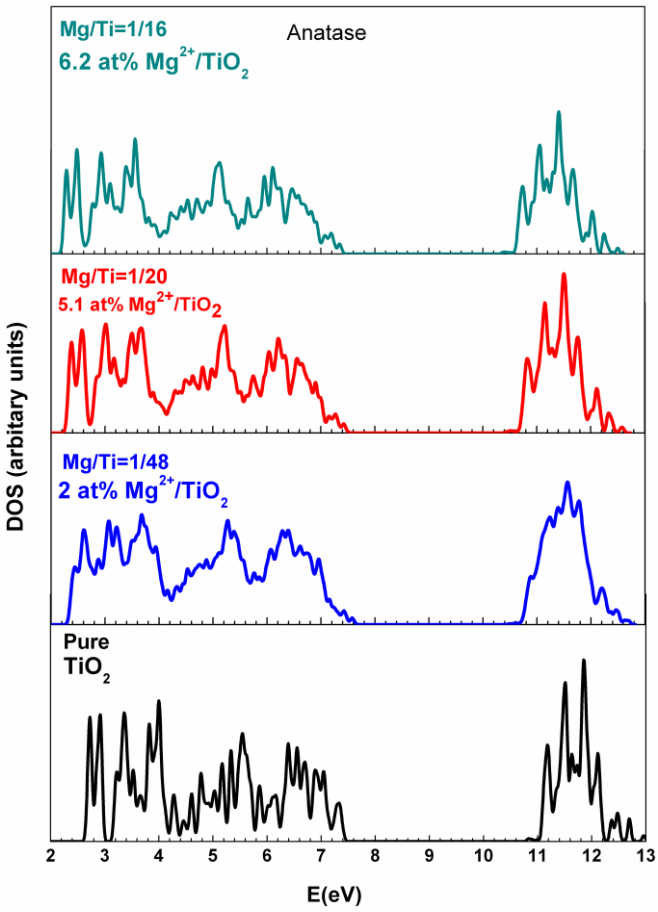

Fig.5. Density of states for the pure and doped anatase samples.

3.5. Photocatalytic activity

The photocatalytic activity of the pure and Mg^{2+} doped TiO_2 anatase samples was evaluated by oxidizing the NO gas as well as decomposing the acetaldehyde gas. In general the photocatalyst is activated by light, in the case of TiO_2 by UV-A irradiation, forming this way an electron and hole pair (e^-/h^+):

$$TiO_2 \xrightarrow{+h\nu} h^+ + e^- \qquad (4)$$

The electron that has migrated to the {101} crystal facets of the TiO_2 anatase nanoplates [12,29] react with the favourably adsorbed O_2 [30] on these specific facets forming superoxide anions (O_2^-):

$$e^- + O_2 \rightarrow O_2^- \quad (5)$$

The superoxide anion O_2^- is a base and will form HO_2 radicals with traces of water that is originated from the humidity of the air flow [31-34]. The HO_2 may recombine to give H_2O_2:

$$2HO_2 \rightarrow H_2O_2 + O_2 \quad (6)$$

or may react with the NO gas, which is adsorbed on the {101} crystal facets of the TiO_2 anatase nanoplates, forming NO_2 and a hydroxyl radical [30,35]:

$$HO_2 + NO \rightarrow NO_2 + OH \quad (7)$$

The products from the above reaction can further react to the end product which is nitric acid (HNO_3):

$$NO_2 + OH \rightarrow HNO_3 \quad (8)$$

All nitrogen species (NO, NO_2) are photocatalytically oxidized leading to nitrate (NO_3^-) where as O_2 is photochemically reduced according to the following chemical reaction:

$$NO + NO_2 + O_2 + H_2O \xrightarrow{TiO_2+hv} 2HNO_3 \quad (9)$$

Previous experimental studies have shown that no photocatalytic decomposition of the NO gas was observed in the absence of O_2, since no HO_2 was formed in nitrogen [35]. Furthermore, it has shown that the first order rate constants for photochemical reactions of NO and NO_2 with TiO_2 are independent of the type of mixture of nitrogen oxides. This means that there is

no inhibition of the decomposition of one compound by the other under experimental conditions applied.

The photogenerated holes that migrate to the {001} crystal facets of the TiO_2 anatase nanoplates react with the dissociated water molecules that are present on these particular facets creating active oxygen species, which have strong oxidative ability for many organic substances [36,37]:

Previous studies have shown that acetaldehyde is photocatalytically degradated either by the OH radicals or by the photogenerated holes according to the following chemical reactions [38-43]:

$$H_2O+h^+ \rightarrow H^+ + OH \quad (10)$$

$$CH_3CHO + OH \rightarrow CH_3CO + H_2O \quad (11)$$

$$CH_3CO + OH \rightarrow CH_3COOH \quad (12)$$

$$CH_3COOH + 2H_2O + 8h^+ \rightarrow 2CO_2 + 8H^+ \quad (13)$$

The previous stoichiometry is adopted with the assumption that the only radical species driving the photocatalytic degradation are the OH and the photogenerated holes. Acetic acid is formed which undergoes further oxidation to CO_2. However, it has been reported that when the number of the photogenerated holes on the TiO_2 surface is much larger than the number of the adsorbed acetaldehyde molecules, the proportion of direct oxidative conversion can be increased [39, 41].

Figure 6 shows the photonic efficiency of the studied samples for NO oxidation and acetaldehyde decomposition. The difference of the electron negativity between Ti and Mg, the Ti-O-Mg formed *via* Mg^{2+} entering into the shallow surface TiO_2 could promote the charges to transfer, resulting in an increase of the photocatalytic activity. Moreover, it is known from the literature

that alkaline-earth metal ion doping causes lattice deformation and thus produces defects in crystals [24]. These defects can inhibit the recombination of electron-hole pairs, resulting in higher photocatalytic activity. As the concentration of the alkaline dopant increases, the interfacial electron and hole transfer are inhibitted, and the photoactivity is reduced. All Mg^{2+} doped nanoplates showed higher or the same photocatalytic activity in decomposing acetaldehyde gas compared to the pure anatase nanoplates due to their dominant {001} facets and their large hole density. The photocatalytic activity in oxidizing the NO gas, was the same for the sample with the smallest amount of Mg^{2+} dopant in comparison to the pure anatase nanoplates. As the concentration of the dopant increased their photocatalytic activity declined.

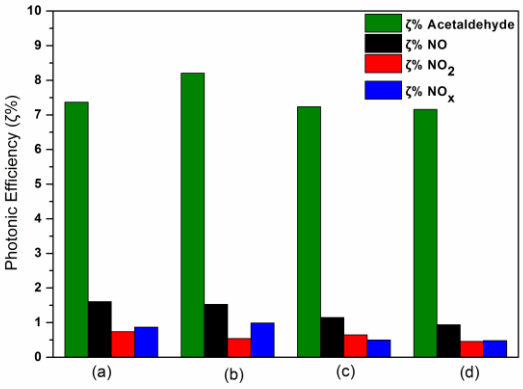

Fig. 6. Photonic efficiency of the pure TiO_2 anatase nanoplates (a), 2 at% Mg^{2+}/TiO_2 (b), 5.1 at% Mg^{2+}/TiO_2 (c), 6.2 at% Mg^{2+}/TiO_2 anatase nanocrystals (d) for NO oxidation and acetaldehyde decomposition.

4. Conclusions

According to the XRD patterns the Bragg peak that corresponds to the (004) reflection of the TiO_2 and Mg^{2+}/TiO_2 samples is broad due to the

anisotropic growth of the nanocrystals along the c-axis of the anatase lattice. This indicates that the c-axis is smaller than the a and b-axis of the anatase lattice and the morphological structure is in the form of plates. TEM observations showed that the {001} facets are dominant in comparison to the {101} facets of the anatase crystal. Magnesium doping in the anatase lattice leads to a different morphological structure where the nanoplates are piled up vertically creating large nanocrystals. As the percentage of the dopant increases the nanocrystals became denser. The incorporation of Mg^{2+} ions into the TiO_2 was evidenced by XPS analysis. The DRS analysis and DFT calculations showed that doping of Mg^{2+} into TiO_2 shifts the absorption band of TiO_2 to lower energy. Magnesium doping in small amounts causes better separation of electrons and holes allowing more efficient channelling to the surface of the nanocrystals of these produced charge carriers into useful redox reactions, thus enhancing the photocatalytic activity in comparison to the pure TiO_2 nanoplates.

Acknowledgements

This work was partially supported by the General Secretariat for Research and Technology of Greece under the project 09SYN-42-925-ARISTON.

References

[1] A. Fujishima and K. Honda, Nature 238 (1972) 37-38.

[2] M. R. Hoffmann, S. T. Martin, W. Choi and D. W. Bahnemann, Chem. Rev. 95 (1995) 69-96.

[3] J. G. Yu, J. J. Fan and K. L. Lv, Nanoscale 2 (2010) 2144-2129.

[4] B. Laskova, M. Zukalova, L. Kavan, A. Chou, P. Liska, Z. Wei, L. Bin, P. Kubat, E. Ghadiri, J. E. Moser, M. Grätzel, J. Solid State Electrochem. 16 (2012) 2993-3001.

[5] D. Q. Zhang, G. S. Li, H. B. Wang, K. M. Chan and J. G. Yu, Cryst. Growth Des. 10 (2010) 1130-1137.

[6]A. Feldhoff, C. Mendive, T. Bredow and D. W. Bahnemann, ChemPhysChem 8 (2007) 805-809.

[7] X. N. Wang, B. B. Huang, Z. Y. Wang, X. Y. Qin, X. Y. Zhang, Y. Dai and M. H. Whangbo, Chem.Eur. J. 16 (2010) 7106-7109.

[8] W. Choi, A. Termin, M. R. Hoffman, J. Phys. Chem. 98 (1994) 13669-13679.

[9] Y. Li, T. Wang, S. Peng, Acta Phys-Chim. Sin. 20 (2004) 1434-1439.

[10] J. Zhao, T. Wu, K. Wu, Environ. Sci. Technol. 32 (1998) 2394- 2400.

[11] V. Subramanian, E. Wolf, P.V. Kamat, J. Phys. Chem. B 105 (2001) 11439-11446.

[12] W. Q. Fang, X. Q. Gong, H. G. Yang, J. Phys. Chem. Lett. 2 (2011) 725–734.

[13] T. Tachikawa, S. Yamashita, T. Majima J. Am. Chem. Soc. 133 (2011) 7197–7204.

[14] Y. F. Li, Z. P. Liu, L. Liu, W. Gao, J. Am. Chem. Soc. 132 (2010) 13008–13015.

[15] P. Hohenberg and W. Kohn, Phys. Rev. 136 (1964) B864-B871.

[16] W. Kohn and L. J. Sham, Phys. Rev. 140 (1965) A1133-A1138.

[17] P. Giannozzi et al., http://www.quantum-espresso.org.

[18] K. A. Brueckner, J. L. Gammel and H. Weitzner, Phys. Rev. 110 (1958) 431- 445.

[19] H. Lin, C. P. Huang, W. Li, C. Ni, S. Ismat Shah and Yao-Hsuan Tseng, Appl. Catal. B: Environ. 68 (2006) 1-11.

[20] ISO/DIS 22197-1 Fine ceramics (advanced ceramics, advanced technical ceramics). Test method for air-purification performance of semiconducting photocatalytic materials. Part 1. Removal of nitric oxide.

[21] M. V. Sofianou, C. Trapalis, V. Psycharis, N. Boukos, T. Vaimakis, J. G. Yu, W. G. Wang, Environ. Sci. Pollut. Res. 19 (2012) 3719-3726.

[22] C. Greaves, J. Appl. Cryst. 18 (1985) 48-50.

[23] J. I. Langford, D. Louër, J. Appl. Cryst. 15 (1982) 20-26.

[24] R. C. Evans, An Introduction to Crystal Chemistry, 2nd Ed, Cambridge Univ. Press, Cambridge, 1964.

[25] Y. X. Li, S. Q. Peng, F. G. Jiang, G. X. Lu, S. B. Li, J. Serb. Chem. Soc. 4 (2007) 393-402.

[26] T. Siva Rao, T. Abdo Segne, T. Susmitha, A. Balaram Kiran, C. Subrahmanyam, Advan. Mater. Sci. Eng. 2012 (2012) 1-9.

[27] P. Peshev, M. Khrussanova, D. Chakarov, M. Terzieva, Ts. Marinova, Mat. Res. Bull. 24 (1989) 207-212.

[28] E. L. Simmons, J. Mod. Opt. 19 (1972) 10 845-851.

[29] T. Tachikawa, S. Yamashita, T. Majima J. Am. Chem. Soc. 133 (2011) 7197–7204.

[30] R. Wanbayor, V. Ruangpornivisuti, J. Mol. Struct –Theochem. 52 (2010) 103-108.

[31] C. Kormann, D. W. Bahnemann, M. R. Hoffmann, Environ. Sci. Technol. 22 (1988) 798-806.

[32] W. Kubo, T. Tatsuma, Anal. Sci. 20 (2004) 591-593.

[33] T. Hirakawal, Y. Nosaha, J. Phys. Chem. C 112 (2008) 15818-15823.

[34] K. Hashimoto, K. Wasada, N. Toukai, H. Kominami, Y. Kera, J. Photochem. Photobiol., A 136 (2000) 103-109.

[35] S. Laufs, G. Burgeth, W. Duttlinger, R. Kurtenbach, M. Maban, C. Thomas, P. Wiesen, J. Kleffmann, Atmos. Environ. 44 (2010) 2341-2349.

[36] H. Einaga. A. Ogata, J. Hazard. Mater. 164 (2009)1236-1241.

[37] S. Matsuda and H. Hatano, Powder Technol. 151 (2005) 61– 67.

[38] T. Sano, N. Negishi, K. Uchino, J. Tanaka, S. Matsuzawa, K. Takeuchi, J. Photochem. Photobiol., A 160 (2003) 93-98.

[39] Z. Y. Liu, X. T. Zhang, S. S. Nishimoto, T. Murakami, A. Fujishima, Environ. Sci. Technol. 42 (2008) 8547-8551.

[40] I. Sopyan, M. Watanabe, S. Murasawa, K. Hashimoto, A. Fujishima, J. Photochem. Photobiol., A 98 (1996) 79-86.

[41] H. M. Hou, H. Miyafuji, S. Saka, J. Mater. Sci. 41 (2006) 8295-8300.

[42] Z. Q. Yu, S. S. C. Chuang, J. Catal. 246 (2007) 118-126.

[43] D. Meroni, S. Ardizzone, G. Cappeletti, C. Oliva, M. Ceotto, D. Poelman, H. Poelman, Catal. Today 161 (2011) 169-174.